Near-field Measurement and Far-field Characterization of a J-band Antenna Based on an Electro-optic Sensing

Near-field Measurement and Far-field Characterization of a J-band Antenna Based on an Electro-optic Sensing

Shintaro Hisatake[1], Yusuke Tanaka[1], Cybelle Belem[2,3,4], Cyril Luxey[3], Frederic Gianesello[4], Guillaume Ducournau [2], Akihiko Hirata[5]

[1] Gifu University, Gifu, Japan, hisatake@gifu-u.ac.jp

[2] Institut d'Electronique, Microe´lectronique et de Nanotechnologies (IEMN), UMR CNRS 8520/Universite´ de Lille, France

[3] Polytech'Lab, Université Nice-Sophia, 06560 Valbonne, France

[4] STMicroelectronics, 850 rue Jean Monnet | 38926 Crolles | France

[5] Chiba Institute of Technology, Chiba, Japan

***Abstract*—In this paper, we present a near-field pattern measurement based on an electro-optic sensing at 300 GHz band. The measurement system is based on a self-heterodyne technique and non-polarimetric frequency down-conversion technique. The far-field radiation pattern of a horn antenna calculated from the measured near-field pattern is compared with far-field pattern measured with a conventional measurement system using open-ended waveguide probe.**

***Index Terms*—antennas, near-field pattern, far-field pattern, THz wave, measurements.**

I. Introduction

Technologies for Terahertz (THz) wireless communications have been significantly improved in the last couple of years. A 2-m transmission with data rates of 100-Gbps has been demonstrated using a 300-GHz fundamental mixer based on 80-nm InP-HEMT technology [1]. Recently, superheterodyne architecture at 300-GHz band using monolithic integrated circuits has been demonstrated with data rates of 60-Gbps at 10m distance [2]. Not only modern semiconductor technology but also antenna technology are key components to realize cost-efficient and easy-to-deploy transceivers at 300-GHz band. Several antennas such as a low-temperature co-fired ceramic (LTCC) horn antenna [3], dielectric lens antenna [4], multilayered stacked patch antenna on quartz associated with a dielectric lens [5] have been tested for THz wireless communications. However, a high-quality beam pattern is critical for high-data-rate transmissions; therefore, many types of array antennas have extensively been studied to implement beamforming and beam-steering at 300-GHz [6-8].

To maximize the link performance, measurement techniques at 300-GHz band are also crucial. In particular, techniques for visualizing the near-field distribution of THz waves and far-field characterization will become important because electromagnetic (EM) waves are used as the beam in this high-frequency region, and the beam quality affects the system performance. In this paper, we demonstrate THz near-field visualization based on an electro-optic (EO) sensing. The EO probes, which consists of an EO crystal attached to the optical fiber, are used instead of an open-ended waveguide probe. The far-field radiation patterns of a horn antenna are calculated from the measured near- field pattern and compared with far-field pattern measured by a conventional far-field pattern measurement system using open-ended waveguide probe and a vector network analyzer (VNA).

II. Near-field Measurement System

Near-field measurement system [9] is based on a non-polarimetric frequency down conversion technique [10] and self-heterodyne technique [11]. Fig. 1 shows the measurement setup. Two free-running 1.55 μm laser diodes (LDs) are used to generate RF signal and LO signal. The frequency of the RF and LO signals are determined by the frequency of the beat signal generated by combining two optical signals. The frequencies of the LDs are set as f_1 and f_2 ($f_2 > f_1$) and combined using PMF couplers. The frequency of the RF signal is $f_{THz}=f_2-f_1-f_s$. Here, an optical frequency shifter (FS) is used to frequency-shift the LD1 (f_1) by fs (100 kHz in this experiment) for self-heterodyne detection. A uni-traveling-carrier photodiode (UTC-PD) is used to convert the optical beat signal to the THz wave. For the LO signal, a beat signal is used as a probe beam for the non-polarimetric EO frequency down-conversion. The IF signal is amplified by the transimpedance amplifier (TIA) and supplied to the lock-in

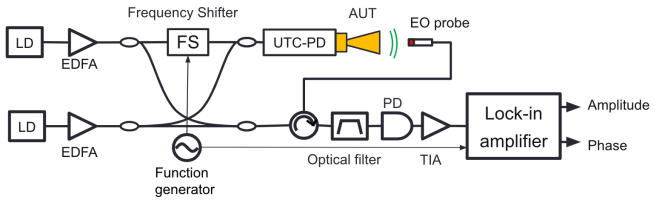

Fig. 1 Near-field measurement setup. LD: laser diode, FS: frequency shifter, UTC-PD: Uni-travelling-carrier photodiode, TIA: transimpedance amplifier.

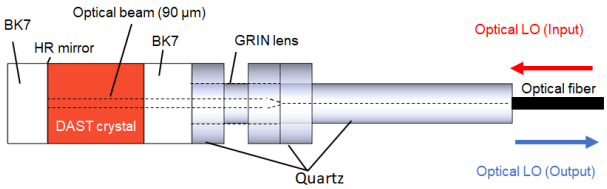

Fig. 2 EO probe. HR mirror: high reflective mirror, GRIN lens: graded-index lens.

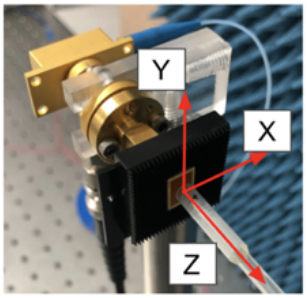

Fig. 3 Photograph of the measured rectangular-type horn antenna and EO probe. The EO probe is covered by a plastic tube. The electromagnetic wave absorber (black) is attached to the horn antenna.

amplifier. The measured amplitude and phase data are acquired by a PC. Although the RF and LO frequency fluctuates, the common-mode frequency fluctuation is cancelled out in the self-heterodyne system, hence amplitude and phase of THz signal can be detected.

In this system, EO probe is used for near-field mapping. As shown in Fig. 2, the sensor head consists of an EO crystal, high-reflection (HR) mirror, spacer, and graded-index (GRIN) lens. The EO crystal is a 4-N, N-dimethylamino-4'-N'-methyl-stilbazolium-tosylate (DAST) crystal. The sensor head is attached to the polarization-maintaining optical fiber (PMF). The GRIN lens collimates the 1.55 μm probe beam (LO signal) transmitted from the PMF. The polarization direction of the probe beam is aligned to the slow-axis of the PMF fiber and the principal dielectric axes of the EO crystal. The diameter of the collimated probe beam in the EO crystal is typically 0.1-0.2 mm, which limits the ultimate spatial resolution. The THz field (RF signal) to be measured interacts with the optical LO (probe beam) in the EO crystal. Then, the probe beam reflected by the HR mirror is focused on the PMF by the GRIN lens.

The THz signal is up-converted to the optical frequency region through the phase modulation of the probe beam in the EO crystal. Then, the generated sideband is down-converted to the IF frequency band by the optical coherent detection. This non-polarimetric frequency down conversion technique solves intrinsic problem of the conventional polarimetric EO detection technique, in which the detection sensitivity fluctuates due to the fiber movement. Also, the EO probe consists of dielectric materials and it does not contain any metallic components, therefore the disturbance to the field is drastically reduced compared with the open-ended waveguide probe. The EO probe is invisible to the near-field and this is one of the advantages of the EO measurement.

Fig. 3 shows a photograph of the horn antenna and EO probe. The EO probe is moved in the XY plane to map the amplitude and phase distribution of the THz wave generated by the UTC-PD. The antenna which emitted the THz wave was a rectangular-type horn antenna. The black part in the photograph is the electromagnetic wave absorber. The electric vector is aligned to the X direction.

III. Experimental Results

Fig. 4 shows the near-field distribution measured on the antenna surface (XY plane). The frequency of the THz wave was 288 GHz. The measured surface was at Z = 2 mm from the antenna surface. The EO probe was moved by 0.1 mm pitch. The time constant of the lock-in detection was 30 ms. The maximum signal-to-ratio (SNR) was about 37 dB. The amplitude data is normalized to its maximum value. The measured area was 12 mm x 12 mm. The measurement time was about 27 minutes.

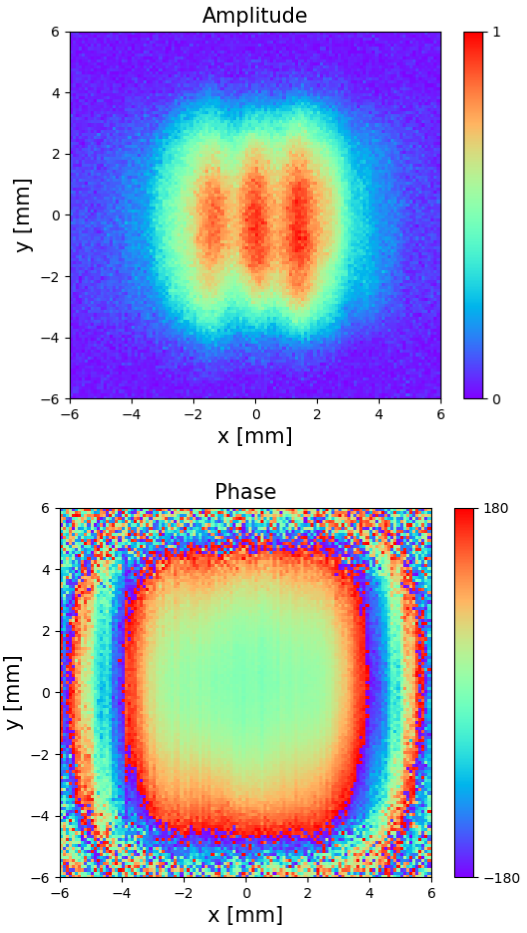

Fig. 4 Measured near-field distribution of the THz wave (288 GHz).

IV. FAR-FIELD CALCULATION

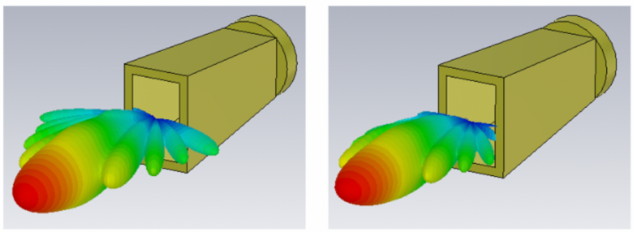

(a) (b)

Fig. 5 Far-field pattern. (a) Simulation, (b) calculated from near-field pattern measured by EO sensing. The horn antenna in this figure is the polygon data used in the simulation, i.e., the 3D simulation model and the experimental results are put together to show the radiation characteristics.

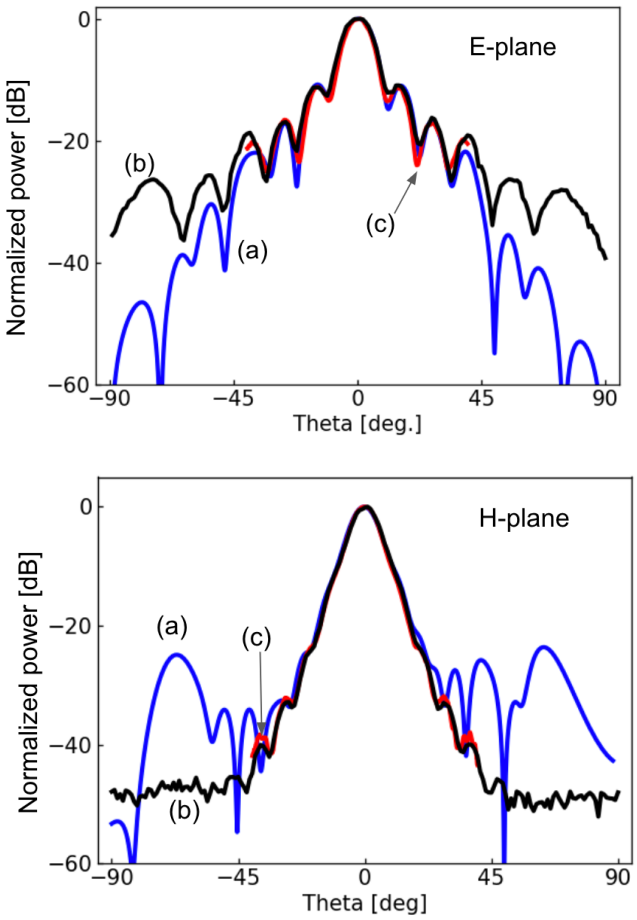

Fig. 6 Experimentally obtained far-field pattern. (a) Calculated from near-field pattern measured by EO sensing (blue), (b) conventional far-field measurement with spherical scanning (black), (c) conventional far-field measurement with planar scanning (red).

Fig. 5 shows the simulated and experimentally obtained far-field patterns calculated from near-field pattern measured by EO sensing. The horn antenna in this figure is the polygon data used in the simulation, i.e., the 3D simulation model and the experimental results are put together to show the radiation characteristics. (Fig. 5 (b)). The far-field pattern was calculated using the CST studio suite. The measured near-field pattern (amplitude and phase) were imported into the CST studio suite and the far-field was calculated. The simulated results were also conducted using the CST studio suite. Fig. 6 shows the experimentally obtained far-field pattern. Lines (a), (b), and (c) are obtained by calculation from near-field pattern measured by EO sensing (blue), conventional far-field measurement with spherical scanning (black), and conventional far-field measurement with planar scanning (red), respectively. The obtained results agreed well with each other in both planes. The deviation at higher spatial frequency region between the results calculated from near-field pattern measured by EO sensing (line (a)) and obtained by the conventional far-field measurement with spherical scanning (line (b)) is due to the limited scanned area of the near-field measurement.

V. CONCLUSION

We demonstrated the near-field measurement of the THz wave transmitted from the horn antenna based on the EO sensing. The three-dimensional radiation pattern calculated from the measured near-field pattern was compared with the simulated results. Also, the far-field pattern in the E-plane and H-plane were compared with the far-field measurement results, showing good agreement between each other. The EO sensing is practical for the THz antenna characterization because of the short measurement time for three-dimensional far-field characterization. The proposed system should be a promising candidate for the high-gain antenna characterization such as the Cassegrain antennas and array antennas.

ACKNOWLEDGMENT

This research is partially supported by funding from Horizon 2020, the European Union's Framework Program for Research and Innovation, under grant agreement No. 814523. ThoR has also received funding from the National Institute of Information and Communications Technology in Japan.

REFERENCES

[1] H. Hamada, T. Fujimura, I. Abdo, K. Okada, H. Song, H. Sugiyama, H. Matsuzaki, and H. Nosaka, “300-GHz 100 Gbps InP-HEMT wireless transceiver using a 300-GHz fundamental mixer,” 2018 IEEE/MTT- S International Microwave Symposium - IMS, June 2018, pp. 1480–1483.

[2] I. Dan, G. Ducournau, S. Hisatake, P. Szriftgiser, R.-P. Braun, I. Kallfass,” A Superheterodyne 300 GHz wireless link for ultra-fast terahertz communication systems,” 2019 European Microwave Conference. IEEE, Oct 2019.

[3] T. Tajima, H.-J. Song, M. Yaita, K. Ajito, N. Kukutsu "300-GHz LTCC horn antennas based on antenna-in-package technology." 2013 European Microwave Conference. IEEE, 2013.

[4] I. Abdo, T. Fujimura, T. Miura, A.Shirane, and K. Okada "A 300GHz dielectric lens antenna," 2019 12th Global Symposium on Millimeter Waves (GSMM). IEEE, 2019.

[5] A. Dyck, M. Rösch , A. Tessmann, A. Leuther , M. Kuri, S. Wagner, B. Gashi, J. Schäfer , and O. Ambacher "A transmitter system-in-package at 300 GHz with an off-chip antenna and GaAs-based MMICs." IEEE Transactions on Terahertz Science and Technology 9.3, 2019, pp. 335-344.

[6] K. Sengupta, and A. Hajimiri, "A 0.28 THz power-generation and beam-steering array in CMOS based on distributed active radiators," IEEE J. Solid-State Circuits, volume 47, issue 12, 3, 2012, pp. 013-3031.

[7] B. Wu, Y. Hu, Y. T. Zhao, W. B. Lu, and W. Zhang “Large angle beam steering THz antenna using active frequency selective surface based on hybrid graphene-gold structure,” Opt. Express, volume 26, issue 12, 2018, pp. 15353-15361.

[8] K. Tekkouk, J. Hirokawa, K. Oogimoto, T. Nagatsuma, H. Seto, Y. Inoue, and M. Saito “Corporate-feed slotted waveguide array antenna in the 350-GHz band by silicon process,” IEEE Trans. Antennas Propag., volume 65, issue 1, 2017, pp. 217-225.

[9] S. Hisatake, "Electrooptic field visualization and its application to millimeter-wave and terahertz antenna characterization," 2017 IEEE Conference on Antenna Measurements & Applications (CAMA), Tsukuba, 2017, pp. 330-333.

[10] S. Hisatake, and T. Nagatsuma, “Nonpolarimetric technique for homodyne-type electrooptic field detection,” Appl. Phys Express, volume **5,** article numeber 1, 2012.

[11] S. Hisatake, G. Kitahara, K. Ajito, Y. Fukada, N. Yoshimoto, and T. Nagatsuma, “Phase-sensitive terahertz self-heterodyne system based on photodiode and low-temperature-grown GaAs photoconductor at 1.55 μm,” IEEE Sensors Journal, Vol. 13, 2013, pp. 31-36.